Gradual development of ammonia-induced syntrophic acetate-oxidizing activities under mesophilic and thermophilic conditions quantitatively tracked using multiple isotopic approaches

Liping Hao, Lu Fan, Olivier Chapleur, Angéline Guenne, Ariane Bize, Chrystelle Bureau, Fan Lü, Pinjing He, Théodore Bouchez, Laurent Mazeas

Gradual development of ammonia-induced syntrophic acetate-oxidizing activities under mesophilic and thermophilic conditions quantitatively tracked by multiple isotopic approaches

Authors: Liping Hao[a,*], Lu Fan[a], Olivier Chapleur[b], Angéline Guenne[b], Ariane Bize[b], Chrystelle Bureau[b], Fan Lü[c], Pinjing He[c,*], Théodore Bouchez[b,*], Laurent Mazéas[b,*]

Affiliation:

[a]State Key Laboratory of Pollution Control and Resource Reuse, Tongji University, Shanghai 200092, China

[b]Université Paris-Saclay, INRAE, PRocédés biOtechnologiques au Service de l'Environnement, 92761 Antony, France

[c]Institute of Waste Treatment & Reclamation, Tongji University, Shanghai 200092, China

*__Correspondence to__: Laurent Mazéas, email: laurent.mazeas@inrae.fr; Théodore Bouchez, email: theodore.bouchez@inrae.fr ; Pinjing He, email: xhpjk@tongji.edu.cn ; Liping Hao, email: 19005@tongji.edu.cn.

Abstract

Insights into microbiota adaptation to increased ammonia stress, and identification of indicator microorganisms can help to optimize the operation of anaerobic digesters. To identify microbial indicators and establish links between their appearance with acetoclastic methanogenesis (AM), syntrophic acetate oxidation (SAO) or hydrogenotrophic methanogenesis (HM), 40 anaerobic reactors fed with acetate of 110 mmol/L were launched at NH_4^+-N concentrations of 0.14 g/L, 5.00 g/L or 7.00 g/L, inoculated with thermophilic or mesophilic microbiota with or without pre-exposure to ammonia stress. Four stable carbon isotope probing strategies were applied in parallel, with [1,2-^{13}C]-CH_3COOH, [2-^{13}C]-CH_3COOH, [^{13}C]$NaHCO_3$ or non-labeled CH_3COOH used individually. The last three settings were used to quantify the methanogenic pathways by tracking labeled ^{13}C or natural ^{13}C signatures in the produced CH_4 and CO_2, which consistently detected the dynamic transition of dominant pathways from AM to SAO-HM under ammonia stress. Quantitative PCR and fluorescence in-situ hybridization recorded the procedure acetotrophic methanogens being outcompeted by acetate-oxidizing syntrophs. The first and last strategies were designed to probe the active acetate-mineralizing microbes with DNA-SIP, which detected known acetate-oxidizing syntrophs like *Syntrophaceticus* and *Methanoculleus*, as well as novel members of *Pseudomona*, *Bacillus* and Symbiobacteraceae. With NanoSIMS, some bacterial cells were observed to be fixing CO_2 from [^{13}C]$NaHCO_3$. In this study, *Methanosaeta* was only active with ammonia < 200 mg-N/L, the syntrophs catalyzing SAO-HM started to compete with AM-conducting *Methanosarcina* at medium-level ammonia of 200-500 mg-N/L, and outcompeted the acetotrophic methanogens with ammonia > 500 mg-N/L. Under ammonia stress, diverse known and novel microbial taxa were involved in acetate mineralization, and are comparable

between individual studies.

Keywords

Stable isotope probing, natural ^{13}C signature, ammonia stress, acclimation, bacterial CO_2 fixation, NanoSIMS

Introduction

During anaerobic digestion (AD), acetotrophic methanogens, syntrophic acetate oxidizing bacteria (SAOB), and hydrogenotrophic methanogens form an essential functional guild, which turns acetate into CH_4 and CO_2 via two different pathways: acetoclastic methanogenesis (AM), or syntrophic acetate oxidation (SAO) followed by hydrogenotrophic methanogenesis (HM). SAOB have been found to replace acetotrophic methanogens as predominant acetate-consumers under conditions

---

Abbreviations

AD: Anaerobic digestion

SAO: Syntrophic acetate oxidation

HM: Hydrogenotrophic methanogenesis

AM: Acetoclastic methanogenesis

SAO-HM: Syntrophic acetate oxidation followed by hydrogenotrophic methanogenesis

SAOB: Syntrophic acetate oxidizing bacteria

FISH: Fluorescence in-situ hybridization

CLSM: Confocal laser scanning microscopy

QPCR: Quantitative polymerase chain reaction

DNA-SIP: Deoxyribonucleic acid-stable isotope probing

NanoSIMS: Nanoscale secondary ion mass spectrometry

including increased levels of ammonia (Hao et al., 2017; Westerholm et al., 2018), elevated temperature (Dyksma et al., 2020; Ho et al., 2013) or increased organic loading rate (Li et al., 2018; Lü et al., 2013), which could be caused by a change in operating conditions or in the period when the reactors were starting up. SAOB grow slowly since very limited energy is shared between the bacteria and methanogen partners in the SAO-HM reaction (Hattori, 2008; Westerholm et al., 2019). Such an adaptation of the microbiota to the changed environment usually results in performance instability or in a long lag phase (Dai et al., 2016). The AD process dominated by SAO-HM usually presents a pseudo-steady state with a relatively low CH_4 production rate and instability (Fotidis et al., 2013b) if the aim of the digester operation is still to optimize AM. A deep understanding of this microbial adaptation procedure would then help to determine the status and to develop tailored operating strategies (Westerholm et al., 2015), such as acclimation (Puig-Castellví et al., 2020) and bioaugmentation (Fotidis et al., 2013a; Westerholm et al., 2012), to enhance the stability, shorten the lag phase and better manage the AD process under stress conditions. To this end, it is crucial to identify the microbial players of the acetate-mineralizing functional guild, and establish reliable links between their roles with SAO, HM or AM pathways.

SAO-HM phenomenon and the relevant functional microorganisms have been studied for two decades, and found to be extensively distributed in full-scale anaerobic digesters operating under high ammonia levels or in thermophilic conditions (Hao et al., 2016; Pan et al., 2020; Sun et al., 2014). Using traditional cultivation methods, to date, only five SAOB have been isolated and characterized, including the mesophilic *Clostridium ultunense* (Schnürer et al., 1996) and *Syntrophaceticus schinkii* (Westerholm et al., 2010), the thermotolerant *Tepidanaerobacter acetatoxydans* (Westerholm et al., 2011), and the thermophilic *Pseudothermotoga lettingae* (Balk et

al., 2002; Bhandari and Gupta, 2014) and *Thermacetogenium phaeum* (Hattori et al., 2000). *Methanoculleus* and *Methanothermobacter* were respectively the coupled H_2/CO_2-consuming methanogens with the first four and the last SAOB in co-culture. Nevertheless, these well-studied SAOB usually display low abundance in the complex microbiota or even cannot be detected in several reactors showing a significant contribution of SAO (Hao et al., 2016; Mosbæk et al., 2016; Puig-Castellví et al., 2020; Werner et al., 2014). High-throughput sequencing-based techniques were used to search for potential SAOB based on the relative abundance of the taxon or on the detection of functional genes (like *fhs*) in specific members (Dyksma et al., 2020; Müller et al., 2013; Nobu et al., 2015). Several attempts were also made to enrich SAOB by incubation with acetate as sole organic carbon source (Dyksma et al., 2020; Li et al., 2009; Wang et al., 2018; Werner et al., 2014; Westerholm et al., 2018; Zheng et al., 2019). Results indicated involvement of diverse novel bacterial taxa, thereby significantly extending the repository of proposed SAOB candidates. However, the phylogenetic relationship between these newly proposed SAOB candidates derived from individual studies is not yet known. It is unclear whether they are widespread or only detected in an isolated study, and if they did catalyze SAO, since synchronous analyses of metabolic pathways and microbial populations were not carried out in some studies. A detailed comparison is thus needed to better interpret the relationship between the diverse SAOB candidates.

In AD systems, AM is mainly catalyzed by methanogens belonging to the genera *Methanosaeta* and *Methanosarcina*. However, some members of the *Methanosarcina* genus can use both acetate and H_2/CO_2 as methanogenic precursors (Thauer et al., 2008). The metabolic type of these populations can sometimes not be clearly distinguished between AM, HM or even SAO (De Vrieze et al., 2012; Dyksma et al., 2020; Hao et al., 2015). Dynamic analyses of metabolic pathways along with changes in the

microbiota can help pinpoint the function of dominant microbial populations in specific circumstance, which could help overcoming the aforementioned problems. CH_4-producing pathways were quantified by tracking stable carbon isotope (^{13}C) released from the methyl-carbon labeled acetate, which was only used *ex situ* in batch incubation (Werner et al., 2014). In addition, apparent ^{13}C fractionation factor (α_c) was used *in situ* to determine the dominant methanogenic pathway in full scale digesters (Hao et al., 2016; Polag et al., 2015), which was calculated by analyzing the natural ^{13}C signature of CH_4 and CO_2 in biogas based on the assumption that the CO_2 precursor for HM comes from the CO_2-carbonate system (Whiticar et al., 1986). The efficiency of α_c to distinguish AM and SAO-HM and the latter assumption need to be confirmed or refined with ^{13}C labeling methods, which are currently lacking.

The aim of this study was thus to quantitatively investigate the dynamic change in AD microbiota with respect to both metabolic pathways and active microbial members, when exposed to ammonia stress in acetate-fed batch reactors. The influence of temperature and acclimation on microbial behavior was studied using high and low levels of ammonia. The inoculating microbiota originated from two anaerobic reactors that were previously shown to be dominated by AM at low ammonia conditions (Hao et al., 2015, 2017). During the process, three different stable isotope labeling strategies were applied in parallel to dynamically quantify the pathways, and to compare the methods; QPCR was used to record the number of major methanogenic populations, and fluorescence in situ hybridization (FISH) with confocal laser scanning microscopy (CLSM) was used to visualize the cell morphologies and distribution; DNA stable isotope probing (DNA-SIP) with simultaneous ^{13}C and ^{15}N labeling was applied to track down the active microbial players, which were further compared with those found in previous studies; nanoscale secondary ion mass spectrometry (NanoSIMS) was used to

observe enrichment of isotope labels in microbial cells. This is the first work to profile the microbial transition under stress using such integrated approaches.

Materials and methods

Inoculating microbiota

Two types of anaerobic sludge biomass were used as the source microbiota. The biomasses originated from, respectively, a mesophilic reactor operated at 35°C (named M) and a thermophilic reactor operated at 55°C (named T). To prepare inocula with and without acclimation, microbiota M and T were pre-incubated with NH_4^+-N of 0.14 g/L, 5.00 g/L (for M) or 7.00 g/L (for T) in basic medium (**Supplementary Section 1.1**) with acetate of 80 mmol/L anaerobically. The inocula resulting from pre-incubation with 5.00 and 7.00 g-N/L were considered as "acclimated" and named "MA" and "TA", while the inocula resulting from 0.14 g-N/L were considered as "non-acclimated" and named "MnA" and "TnA" (**Figure 1**). When methane production ceased after 32 days (**Figure S1**), the microbial solids were collected by centrifugation at 8 000 g for 5 min and used as inoculating microbiota at a concentration of 4.00 g/L of volatile solids in further batch experiments.

^{13}C and ^{15}N labeling experiment

The four different inocula were then respectively incubated at "Low" (0.14 g-N/L) and "High" (5.00 g-N/L for M or 7.00 g-N/L for T) ammonium levels in 327-mL serum bottles (Fisher Scientific), resulting in eight sets of anaerobic reactors (**Figure 1, Table S1**). The "High" NH_4^+-N concentrations were used to initiate a shift in the predominant pathway under mesophilic and thermophilic conditions respectively, as demonstrated previously (Hao et al., 2017). NH_4Cl was added as a source of ammonia stress and nitrogen for microbial growth. Acetic acid (110 mmol/L) was used as the sole organic

carbon source. $NaHCO_3$ (140 mmol/L) and K_2CO_3 (20 mmol/L) were added to provide buffering capacity. Each set included five reactors (r1-r5) with different carbon and nitrogen isotope-labeling strategies: r1 and r2 were run without any ^{13}C- or ^{15}N-labeled compounds, r3 was fed with [2-^{13}C]CH_3COOH (99%, Sigma), r4 with [1,2-^{13}C]CH_3COOH (99%, Sigma), r5 with 50% of [^{13}C]$NaHCO_3$ (98%, Isotec), and all three with [^{15}N]NH_4Cl (99%, Sigma). Therein, reactors r3 and r5 were set to quantify the contribution of AM or SAO-HM to acetate mineralization, by monitoring ^{13}C flow to CH_4 and CO_2 in the biogas; r4 was set for DNA-SIP to track the active microbial members assimilating ^{13}C from acetate; r1 and r2 served as control for DNA-SIP and to evaluate CH_4-production pathways by analyzing the natural ^{13}C signature of biogas.

r1-r4 and r5 were filled with respectively 73 mL and 63 mL of basic medium with addition of acetate, NH_4Cl and (bi)carbonates. The initial pH was adjusted to 6.5 (±0.1) with 1.0 mol/L HCl, and kept below 8.5 throughout incubation. The headspace was filled with N_2 gas. Reactors inoculated with MA and MnA or TA and TnA were incubated at 35 ℃ or 55 ℃ statically. During incubation, gas and liquid samples were taken periodically using syringes, and stored for further analyses.

CH_4 production and ammonia calculation

CH_4 yield was calculated by monitoring the gas pressure and CH_4 composition in the headspace as described previously (Hao et al., 2017).The modified Gompertz three-parameter model was fitted to the cumulative CH_4 yield curve of each reactor (Zwietering et al., 1990). Simulated CH_4 yield and production rates for each day were then predicted from the fitting curves. The pH and the acetate concentration in the liquid phase were analyzed as detailed previously (Hao et al., 2017). The concentration of free ammonia (NH_3) was calculated by considering the pH, temperature and total ammonium (NH_4^+) concentration (Hao et al., 2015). Details are provided in

Supplementary Sections 1.2-1.4.

Contribution of the SAO-HM pathway quantified with ^{13}C in the biogas

The natural ^{13}C signature of CH_4 ($\delta^{13}CH_4$) and CO_2 ($\delta^{13}CO_2$) was analyzed in reactors r1 and r2, and ^{13}C composition of CH_4 ($\Delta^{13}CH_4$) and CO_2 ($\Delta^{13}CO2$) was analyzed in reactors r3 and r5, as detailed in **Supplementary Section 1.2**. The latter was used to calculate the percentage contribution of pathways SAO-HM ($f_{SAO\text{-}HM}$) and AM (f_{AM}) based on the source of carbon used to produce CH_4 and CO_2. In the SAO-HM pathway, acetate is oxidized to H_2 and CO_2, the resulting H_2 then reduces CO_2 to CH_4. The CO_2 precursor is assumed to originate from the $CO_3^{2-}/HCO_3^{-}/CO_2$ system. Conversely, in the AM pathway, carbon in CH_4 only originates from the methyl-group of CH_3COO^{-}. Therefore, in reactor r3 with [2-^{13}C]CH_3COOH, $\Delta^{13}CH_4$ is calculated as:

$$\Delta^{13}CH_4 = 100\% \times f_{AM} + \Delta^{13}CO_2 \times f_{SAO\text{-}HM} \quad \textbf{(Eq.1)}$$

and $f_{SAO\text{-}HM}$ is calculated as:

$$f_{SAO\text{-}HM} = (100\% - \Delta^{13}CH_4) / (100\% - \Delta^{13}CO_2) \times 100\% \quad \textbf{(Eq.2)}$$

In reactor r5, [^{13}C]$NaHCO_3$ is the sole ^{13}C source, and $^{13}CH_4$ can be only generated via SAO-HM, thus $\Delta^{13}CH_4$ is calculated as:

$$\Delta^{13}CH_4 = \Delta^{13}CO_2 \times f_{SAO\text{-}HM} \quad \textbf{(Eq.3)}$$

and $f_{SAO\text{-}HM}$ is calculated as:

$$f_{SAO\text{-}HM} = \Delta^{13}CH_4 / \Delta^{13}CO_2 \times 100\% \quad \textbf{(Eq.4)}$$

In reactors r1 and r2, α_C is calculated with the natural ^{13}C signature as follows (Whiticar et al., 1986):

$$\alpha_C = (\delta^{13}CO_2 + 10^3) / (\delta^{13}CH_4 + 10^3) \quad \textbf{(Eq.5)}$$

FISH-CLSM and FISH-NanoSIMS

Biomass samples were fixed for FISH analysis as described previously (Daims et al., 2005). Probes EUB338, ARC915, MX825, MS1414 and MG1200 were used to target respectively, Bacteria, Archaea, Methanosaetaceae, Methanosarcinaceae, and Methanomicrobiales, which were labeled with fluorescent dyes, and the signals were observed with CLSM. FISH-NanoSIMS was used to compare the spatial location of ^{13}C and ^{15}N to the brominated bacterial probe EUB338. Cell isotopic enrichment was calculated as described previously (Chapleur et al., 2013). Details are given in **Supplementary Sections 1.5-1.6**.

QPCR, DNA-SIP and pyrosequencing

DNA was extracted from liquid aliquots sampled periodically from the reactors, and used as templates for QPCR to quantify total bacteria and the different methanogen populations. DNA samples derived from reactors r4 and r1 (or r2) with and without $^{13}C/^{15}N$ labeling were used for DNA-SIP. Based on the CsCl buoyant density gradient, total DNA was separated into heavy and light fractions that were respectively collected and used for pyrosequencing. Primer pairs 349F/806R and 28F/519R were used to target Archaea and Bacteria. The sequences were further analyzed with Qiime software, and taxonomic classification of the generated OTUs was conducted with qiime 2's q2-feature-classifier plugin (Bokulich et al., 2018) based on the Silva SSU database, version 138.1. Several OTUs enriching ^{13}C from acetate were selected to compare with potential SAOB proposed in previous studies. The raw reads have been deposited in European Nucleotide Archive under the project ID PRJEB44265. Details are provided in **Supplementary Sections 1.7-1.11**.

Results

Acetate to methane: the transformation procedure differed

The added acetate was consistently converted into CH_4 in about 10 days in all the reactors containing NH_4^+-N of 0.14 g/L (low). This conversion procedure differed in reactors with NH_4^+-N of 5.00 g/L or 7.00 g/L (high) (**Figure 2**). For the non-acclimated microbiota, a first active CH_4-production period was followed with an intermediate lag phase of 11-55 days with no obvious generation of CH_4, after which methanogenic activity recovered. TnA also displayed an initial lag phase of ~23 days before the first active period. For the acclimated microbiota, MA demonstated low methanogenic activity in the first period of 50-60 days, after which CH_4 production became quite active. TA behaved slightly differently, with an initial lag phase of 20-30 days followed by high methanogenic activity. In the five reactors operated in parallel, some variations in the methanogenesis recovery speed were observed, especially for MA.

Multiple isotope-tracking approaches quantitatively recorded the gradual involvement of the SAO pathway

Three ^{13}C-tracking approaches were used to quantitate the contribution of the SAO-HM pathway by tracking ^{13}C flow into CH_4 and CO_2 of biogas from [2-^{13}C]CH_3COOH (in reactor r3) or [^{13}C]$NaHCO_3$ (in reactor r5), and by monitoring the natural ^{13}C signature of biogas (in reactors r1 and r2). The detected ^{13}C contents in CH_4 and CO_2 are illustrated in **Figure 3a-l**. As can be seen in **Figure 3m-p**, $f_{SAO\text{-}HM}$ caculated from $\Delta^{13}CH_4$ and $\Delta^{13}CO_2$ was quite similar in reactors r3 and r5. With a low level of ammonium, CH_4 was mainly produced via the AM pathway with $f_{SAO\text{-}HM}$ generally <10%. With a high level of ammonium, $f_{SAO\text{-}HM}$ gradully increased from <10% in the initial period to 80%-100% when methanogenesis recovered from the lag phase. In the

later period, thermophilic microbiota demonstrated higher $f_{SAO\text{-}HM}$ values (100%) compared with mesophilic microbiota (80%-90%), and ^{13}C composition in CH_4 ($\Delta^{13}CH_4$) and CO_2 ($\Delta^{13}CO_2$) started to overlap (**Figure 3b,d,f,h**), suggesting that carbon in the CH_4 produced comes from a balanced CO_2/bicarbonate/carbonate system that reached equilibrium between the gaseous and liquid phases.

α_C was calculated from $\delta^{13}CH_4$ and $\delta^{13}CO_2$ in reactors r1 and r2. Higher α_C values generally suggest higher contribution of HM, with 1.065 used as a boundary to define predominance of the HM pathway (Conrad, 2005). **Figure 3q-t** shows that, with a low level of ammonium, α_C gradually decreased from 1.066 to 1.028 during the active CH_4-production period, indicating a higher contribution of the AM pathway. With high levels of ammonium, α_C values of non-acclimated microbiota were 1.077-1.051 for TnA, and 1.048-1.041 for MnA in the first active CH_4-production period, and increased to 1.090-1.102 when methanogenesis recovered from the intermediate lag phase, demonstrating the predominant pathway shifted to SAO-HM. The acclimated microbiota behaved differently: TA displayed α_C values of around 1.070 in the initial lag phase and the values increased to 1.094 when methanogenesis became quite active, showing predominance of SAO-HM throughout; MA displayed α_C values that mostly fluctuated between 1.062 and 1.040 in the slow and active CH_4 production periods, revealing a higher contribution of AM.

When compared, most r1 and r2 reactors showed a similar trend to that observed in reactors r3 and r5 when the competition between AM and SAO-HM was quantified, proving that α_C can be used to efficiently monitor the change in the pathway that occurs during acetate transformation into CH_4. Neverthless, parallel MA reactors with high levels of ammonium differed in their metabolic pathways: reactors r3 nd r5 demonstrated a gradually increasing contribution of SAO-HM to 80%-90%; reactors r1

and r2 displayed a mixture of the two pathways with AM sometimes contributing more, which could be due to the different changes in microbial composition.

Visualizing the gradual development of acetate-oxidizing syntrophs

16S rRNA gene copy numbers of major methanogenic members and total bacteria were analyzed with QPCR, including the genera *Methanosarcina* (Family Methanosarcinaceae) and *Methanoculleus* (Order Methanomicrobiales), the family Methanosaetaceae and the order Methanobacteriales (**Figure 4, Figure S2**). The number of *Methanoculleus* increased three-fold in most reactors with a high level of ammonium when methanogenesis recovered from the lag phase, i.e. from the initial 10^3 copies/ng-DNA to 10^6 copies/ng-DNA. But in MA-H-r4, there was only a two-fold increase to 10^5 copies/ng-DNA. Growth of *Methanosarcina* in mesophilic microbiota differed, either increasing from 10^2 to 10^6 or 10^5 copies/ng-DNA in MA-H-r4 or MA-H-r5 and MnA-H-r5, or did not change much in MnA-H-r4. In thermophilic microbiota, *Methanosarcina* and Methanosaetaceae both underwent a one-fold decrease after 100-day incubation in treatments with a high level of ammonium. However, no notable change was observed in Methanobacteriales, which may be not active in this condition (**Supplementary Section 2.1**).

The appearance of methanogens and bacteria was recorded in FISH images (**Figure 5**, **Figure S3**). Initially, mesophilic and thermophilic microbiota were respectively dominated by the rod-shaped cells of Methanosaetaceae and large cell aggregates of Methanosarcinaceae. The signal emitted by these cells was gradually quenched under high-ammonium conditions, and was replaced by the appearance of cell clusters of Bacteria and Methanomicrobiales. Bacterial cells in mesophilic reactors were of different shapes, including rods (2-5 μm in length and around 0.5 μm in width) and a bamboo-like cascade of short rods (**Figure S3w**). In thermophilic reactors, bacterial

cells were longer rods (5-10 μm in length and around 0.5 μm in width). These differences showed that different bacterial taxa were growing under different conditions. Cells of Methanomicrobiales displayed cocci with a diameter of ≤ 1 μm in both conditions, and were loosely assembled with Bacteria. Cell aggregates of Methanosarcinaceae of different sizes (3-20 μm in diameter) appeared in most mesophilic reactors containing a high level of ammonium, but were absent in MnA-H-r4 and MnA-H-r1 (**Figure S3, DataS1**).

Both QPCR and FISH results revealed that, changes in mesophilic microbiota diverged under ammonia stress due to the different extent of the involvement of *Methanosarcinaceae*, which could explain the difference in the speed of recovery of methanogenesis and in the composition of the pathways in parallel reactors. We observed that when methanogenic activity recovered, the abundance of either *Methanosarcina* or *Methanoculleus* reached a similar level (10^6 copies/ng-DNA) to that of the initially dominating Methanosaetaceae (in mesophilic microbiota) or *Methanosarcina* (in thermophilic microbiota). The lag phase before this methanogenic recovery was about 10 days shorter when large aggregates of Methanosarcinaceae cells appeared (**DataS1**), suggesting a higher growth rate of Methanosarcinaceae compared with that of acetate-oxidizing syntrophs. Such microbial divergence phenomena have previously been observed when stress factors occurred and affected the microbiota in the reactors (Goux et al., 2015; Westerholm et al., 2018). In the present study, it seems that ammonia stress may have added further stochasticity to changes in microbial community structure (De Vrieze et al., 2020), which requires further investigation.

Quantification of the influence of free ammonia

Dynamic changes in methanogenic activities could be due to interactions between the functional microbial players and changing environmental factors. As shown in

Figure S4a, alongside increased methane production, the pH gradually increased due to consumption of CH_3COO^-, leading to further transformation of NH_4^+ into NH_3. In mesophilic conditions, the concentration of NH_3 increased from 25 to 519 mg-N/L in reactors with a high level of ammonium, but to less than 31 mg-N/L in reactors with a low level of ammonium. In thermophilic conditions, the values were 50 to 2 106 mg-N/L in reactors with a high level of ammonium, and < 50 mg-N/L in reactors with a low level of ammonium. $f_{SAO\text{-}HM}$, which could also be considered as a percentage of inhibited AM, changed with the concentration of NH_3 in a way like the dose-response model: $f_{SAO\text{-}HM}$ started to increase significantly at an NH_3 concentration of around 200 mg-N/L, and reached 100% when the level of NH_3 exceeded ~500 mg-N/L (**Figure S4b**). The change in α_C with NH_3 showed a similar concomitant increasing trend: when the NH_3 concentration was higher than 200 mg-N/L, α_C values >1.065 started to appear; and when the NH_3 level exceeded ~500 mg/L, α_C value increased to >1.075. Likewise, the number of *Methanoculleus* displayed a 2-3 log-fold increase when NH_3-N exceeded 200 mg/L, similar with *Methanosarcina* in some of the mesophilic reactors. Therefore, the increasing NH_3 concentration probably triggered the replacement of acetotrophic methanogens by acetate-oxidizing syntrophs.

Involvement of diverse bacterial and archaeal members found via DNA-SIP

To identify microorganisms that actively assimilate acetate, the microbiota was incubated with [1,2-^{13}C]CH_3COOH and [^{15}N]NH_4Cl or un-labeled compounds. Total DNA was extracted from samples taken when methanogenesis actively recovered from inhibition, and was further separated into different fractions based on buoyant density (**Figure S5**). As detailed in **Supplementary Section 2.2**, DNA fractions enriched with ^{13}C and ^{15}N were clearly separated from fractions without, thereby guaranteeing isolation of metabolic-active microorganisms. Bacteria and Archaea compositions were

analysed in both heavy and light DNA fractions that represent active and inert microbial consortia, respectively.

Figure 6a,b shows that, in thermophilic microbiota, bacterial members of the genus *Syntrophaceticus* (OTUs 213, 281, 128, 164, 294), the genus *Bacillus* (OTUs 296, 609), and archaeal members of the genus *Methanoculleus* (OTUs 77, 0, 36, 35, 19) were much more abundant (mostly >10 fold higher) in the heavy DNA than in the light, implying potential syntrophism between *Syntrophaceticus* (and/or *Bacillus*) with *Methanoculleus*. By contrast, in mesophilic microbiota, bacterial taxa other than *Syntrophaceticus* were significantly enriched in ^{13}C and ^{15}N, including members of the genus *Pseudomonas* (OTU 292), the genus *Bacillus* (OTU 296) and the family Symbiobacteraceae (OTUs 421, 40). Additionally, various archaeal members of the genus *Methanoculleus* (OTUs 77, 39, 41, 2, 0, 36, 35, 19), RumEN_M2 (OTU 2, belonging to the family Methanomethylophilaceae) and the genus *Methanosarcina* (OTU 81) were more abundant in heavy DNA, indicating involvement of diverse bacterial and archaeal taxa in acetate mineralization.

In addition to temperature, acclimation was shown to have some influence on the composition of active microbial communities. For instance, the OTUs of *Syntrophaceticus* dominated in TnA(-H-r4) and TA(-H-r4) differed. Uncultured Symbiobacteraceae mainly appeared in MnA(-H-r4), while *Methanosarcina* (OTU81) was detected in MA(-H-r4), but not in MnA(-H-r4), as also observed with QPCR and FISH analyses.

These OTUs represented the predominant active microbial players (relative abundance >1%). Among them, only the five OTUs of the genus *Syntrophaceticus* detected in thermophilic microbiota shared 95%-96% similarity with *S. schinkii*, and none of the others exactly matched the well-studied SAOB. Further investigation of the

less abundant OTUs (<1%) detected *T. acetatoxydans* in the heavy DNA from TnA (OTU18, relative abundance 0.3%). OTU107 and OTU542 of the genus *Tepidanaerobacter* both increased 10-fold in the heavy DNA compared with in the light DNA from TnA (0.05% to 0.49%) and MA (0.1% to 0.9%) respectively (**Figure 6c, DataS2)**. Members of genera *Alkaliphilus* and DTU014 have already been described as potential SAOB, as they encode genes that are essential for SAO and were found to be highly abundant in high-ammonia anaerobic digesters (Dyksma et al., 2020; Mosbæk et al., 2016a; Müller et al., 2016). In the present study, OTU532 of the genus *Alkaliphilus* increased markedly in the heavy DNA compared with in the light DNA from MnA (0.03% to 0.36%) and TA (0 to 0.15%); and three OTUs of DTU014 (OTUs35, 83, 563) mainly appeared in the heavy DNA from TnA (≤0.56%). These OTUs can be considered as relatives of known or candidate SAOB. Their appearance at such low abundance probably cannot explain all the SAO activities, especially in MnA where SAO-HM contributed 90% to methane production in the late period.

Evidence for CO_2-fixing bacteria provided by NanoSIMS

Various novel bacterial taxa were found to be involved in acetate mineralization process, which could be assimilating acetate or the produced metabolites like formate and CO_2. To check whether CO_2 could be one of the carbon sources, the microbiota incubated with [^{13}C]$NaHCO_3$ was sampled after 81 days and analyzed using NanoSIMS. **Figure 7** and **Figure S10** shows rod-shape bacterial cells enriched in ^{13}C and ^{15}N at maximum values of 7.0% and 91.0% respectively, values that were 8.0% and 91.0% for the adjacent spherical cells of Methanomicrobiales. These ^{13}C-enrichment values in the biomass were similar to the values of $\Delta^{13}CO_2$ (8.9%) and $\Delta^{13}CH_4$ (8.1%) at the time. This is evidence that some bacteria were actively fixing inorganic carbon when using NH_4^+-N as nitrogen source.

Discussion

Multiple isotope-tracking approaches can quantify acetate-mineralizing pathways

In this study, for the first time, four different ^{13}C and ^{15}N labeling strategies were applied in parallel, and quantitatively tracked both the metabolic pathways and the active microbial players during acetate conversion into CH_4. Our results show that using [2-^{13}C]CH_3COOH and [^{13}C]$NaHCO_3$ led to the same conclusion. When acetate was thoroughly converted via the SAO-HM pathway, $\Delta^{13}CH_4$ values started to overlap with $\Delta^{13}CO_2$, indicating that CO_2, the HM precursor, was derived from the balanced CO_2/bicarbonate/carbonate system. Therefore, analyzing ^{13}C flow from ^{13}C-labeled carbonate/bicarbonate can be used as an alternative method to accurately quantify the contribution of the SAO pathway to acetate conversion, especially when considerable amounts of residual acetate exist in the target system that could dilute the ^{13}C-labeled acetate. Results obtained using natural ^{13}C fractionation generally demonstrated a similar trend to that using ^{13}C labeling approaches. We observed differences between αc values derived from AM ($\geq$1.000) and SAO-HM ($\leq$1.102) as high as 0.102, enabling us to clearly monitor the gradual change in the methanogenic pathways using the natural ^{13}C signature. But it should be noted that a gradual decrease in the αc value (within a narrow range) was observed alongside a rapid degradation in acetate at relatively low levels of ammonia. However, this might not be a sign of increasing AM contribution, as $f_{SAO\text{-}HM}$ was shown to be stable at low values (<10%) by the isotope-labeling methods applied in parallel. This decrease may be related to the change in the isotopic composition of the remaining acetate pool, which became increasingly enriched in ^{13}C during the conversion process. Such result should thus be intepreted with caution.

Appearance of "novel" bacterial and archaeal members in acetate enrichments

Novel bacterial taxa Acetate-fed batch incubation under high levels of ammonia enriched diverse bacterial and archaeal taxa that mineralized acetate mostly via the SAO-HM pathway. The thermophilic microbiota was dominated by various taxa of *Syntrophaceticus* and *Methanoculleus*, the two most commonly found genera forming acetate-oxidizing syntrophs in high-ammonia AD. But in mesophilic microbiota, the known SAOB or reported candidates only accounted for < 3% of enriched bacterial communities, instead, novel members of *Pseudomonas*, *Bacillus*, and uncultured Symbiobacteraceae, which have not yet been shown to possess SAO capability, were actively involved.

Nevertheless, such observations have been reported in previous studies. We thus conducted a comparison focusing on these novel microbial taxa between our work and four other acetate-enrichment experiments performed individually (**Supplementary Sections 1.8-1.9**). Results showed that members of these genera were also abundant in other acetate enrichments. For instance, *Pseudomonas* was enriched with acetate in batch incubation (Dyksma et al., 2020; Li et al., 2009; Werner et al., 2014) or chemostat (Westerholm et al., 2018) from microbiota originated from thermophilic or mesophilic digesters treating various organic wastes, with NH_4^+-N ranging from 0.26 g/L to 5.00 g/L. Nine relevant OTUs were selected from the five studies, the abundance of which was mostly >1% in the microbial communities. Their representative sequences shared from 88.9% to 99.6% similarity, and were assigned to the genera *Pseudomonas* and *Thiopseudomonas* of the family Pseudomonadaceae (**DataS3)**. These results suggest that various *Pseudomonas* members and close relatives are widespread in AD and can be enriched with acetate. Therein, the four representative sequences >1 000 bp, were mostly related to *Pseudomonas* sp. M-08 (AB567742) and *Pseudomonas* sp. Hy-14 (EU620679.2) with ~97% similarity (**Figure S8**), both were denitrifying bacteria

isolated from activated or anaerobic sludge rich in ammonia (Xiao et al., 2009). It is not sure if they are involved in the nitrogen cycle (like anaerobic ammonium oxidation), as no nitrate/nitrite was initially added in our study.

Members of uncultured Symbiobacteraceae and *Bacillus* were also abundantly detected in studies by (Westerholm et al., 2018) and (Dyksma et al., 2020). Typical Symbiobacteraceae species were described to be anaerobic chemo-organotrophic bacteria, utilizing sugars with nitrate as electron acceptor or peptone alone (Shiratori-Takano et al., 2014). Among them, *Symbiobacterium thermophilu*m require an external source of CO_2 or bicarbonate for growth as this bacterium lacks carbonic anhydrase, and is usually found in co-culture with *Geobacillus stearothermophilus* (previously considered as *Bacillus*). *G.stearothermophilus* could provide *S. thermophilu*m with CO_2 and other growth factors (Watsuji et al., 2006). OTUs of *Bacillus infernus,* in our work, were only found in thermophilic conditions (**Figure S7**) like in the study by (Westerholm et al., 2018). As described previously, thermophilic anaerobic species can make respiratory use of formate with electron donors like MnO_2, Fe^{3+} and nitrate (Boone et al., 1995). However, other OTUs of *Bacillus* were found in mesophilic microbiota.

CO_2 fixation by bacteria Even though diverse bacterial members were enriched in isotope-labeled DNA, the actual carbon source and energy metabolism of the novel members still could not be determined. Some of the bacterial cells were observed to be assimilating CO_2 in MA-H-r5 with [^{13}C]$NaHCO_3$. They enriched ^{13}C and ^{15}N to similar levels to that in the adjacent *Methanoculleus*-like cells, showing that the growth rates of these bacteria and of the CO_2/H_2-metabolizing methanogens were similar. Bacterial CO_2 fixation is not rare. As previously reported, *Bacillus subtilis* W23 was observed to incorporate 5% to 6% of $^{13}CO_2$ into microbial biomass during heterotrophic growth,

reflecting biomass formation involving anaplerotic carboxylation of pyruvate (Spona-Friedl et al., 2020). Likewise, *S. thermophilum* (Watsuji et al., 2006) and *Bacillus anthracis* (Eastin and Thorne, 1963) were shown to be able to fix external CO_2, and *Pseudomonas* members had ever been detected in CO_2 enrichments (Jeon et al., 2012). Therefore, CO_2 fixation could be one of the ways that make some novel bacterial taxa appear in heavy DNA, via some as yet unidentified catabolic or anabolic pathways. This result showed that, DNA-SIP only using ^{13}C-labeled acetate cannot fully distinguish the metabolic functions of all the probed microbial members during acetate mineralization. To solve this problem, further investigation is needed by incubation with a series of labeled substrates including acetate, formate and carbonates, or by using meta-omic approaches to pinpoint the active pathways. Even though ^{13}C-labeled carbonate was used in the present study, unfortunately, only samples from ^{13}C-labeled acetate were preserved for DNA-SIP analysis, so we missed the opportunity to distinguish microorganisms assimilating acetate or carbonate/CO_2.

Diverse methanogens involved. All the 19 OTUs of *Methanoculleus* were enriched in heavy DNA, indicating active H_2/CO_2-driven methanogenic activities in the reactors we tested. Especially in MnA-H-r4, TA-H-r4 and TnA-H-r4, *Methanoculleus* contributed to >78% of the archaeal sequences derived from heavy DNA. These OTUs shared 93% to 99% similarity with *Methanoculleus bourgensis*, a common partner of SAOB. Acetotrophic *Methanosaeta* also appeared in heavy DNA, but in smaller quantities than in light DNA; in FISH images, the cells were observed in the initial slow-methane-production period. OTU68 close to *Methanosarcina thermophile* and OTU81 distantly related to known *Methanosarcina* species (**Figure S9**), were respectively detected in thermophilic and mesophilic microbiota. In FISH images, the former was only observed at the beginning of incubation in thermophilic reactors, while

the latter was observed when methanogenic activities recovered from the lag phase in mesophilic reactors. These *Methanosaeta* and *Methanosarcina* members are hypothesized to be responsible for the AM activities that occurred in the initial period of incubation or co-occurred with SAO-HM in the recovery period in mesophilic conditions, as revealed using multiple isotope-tracking approaches. RumRn_M2, a methylotrophic methanogen, was surprisingly enriched in heavy DNA, which has also been found in mesophilic acetate-fed chemostats (Westerholm et al., 2018). As RumRn_M2 members displayed heterotrophic growth on acetate (Söllinger et al., 2016), in the present study, they might have been using acetate as carbon source, and were thus probed with isotopes.

Pre-acclimation accelerated appearance of stress-tolerant microbial players

In our work, the microbiota was considered to be "acclimated" by pre-exposure to ammonia stress for a 32-day period before being used as inoculum, whereas the "non-acclimated" did not undergo a pre-attack of ammonia stress. The acclimated microbiota developed stress-tolerant microbial populations faster, and methanogenic activities were recovered sooner after the lag phase which was 18-46 days shorter than that of the non-acclimated microbiota (**DataS1**). The active microbial members were however more concentrated in a few OTUs, showed less diversity and evenness than that of the non-acclimated. Such differences could be attributed to the impaired activity of the acetotrophic methanogens during pre-exposure to ammonia stress, when they were the major acetate consumers (**Figure S1**). Such an injury not only slowed down AM reaction in the initial period of the batch tests, but also hindered the increase in pH and in the concentration of NH_3 due to consumption of CH_3COO^-. This provided a relatively stable and less-stressful environment for the growth of ammonia-tolerant microorganisms, like *Methanosarcina* or SAOB coupled with *Methanoculleus*. Such

populations probably already started to grow during the acclimation period, and were added to the batch incubation as "seeds", but the amounts must have been very low as no significant difference was observed between "acclimated" and "non-acclimated" inocula with QPCR, due to the fact that acetate in pre-incubation was mainly converted via the AM pathway.

AM-catalyzing *Methanosarcina* tolerant to medium-level ammonia stress

Methanosarcina was repeatedly seen to be active in AD with a medium level of ammonia (100-500 mg-N/L) (Dai et al., 2016; De Vrieze et al., 2012; Fotidis et al., 2013b; Hao et al., 2015). It is however unclear which metabolism they catalyze, since some of the members are mixotrophic or can even use the electrons directly (Rotaru et al., 2017). In this study, *Methanosarcina* cell aggregates appeared in most mesophilic reactors when ammonia level increased to 200-500 mg-N/L. At the same time, Methanosaetaceae members were failed to be observed with FISH-CLSM, which may have lost their activities. *Methanosarcina* are thus hypothesized to be responsible for the concomitant AM pathway that contributed >10% to methane production. In thermophilic reactors, *Methanosarcina* was observed initially when the AM pathway predominated, but was gradually outcompeted by the hydrogenotrophic *Methanoculleus* when ammonia concentration exceeded ~500 mg-N/L. Therefore, *Methanosarcina* mainly catalyzed AM at low (<200 mg-N/L) to medium levels (200-500 mg-N/L) of ammonia. Generally, AM demonstrated higher reaction rates than SAO-HM as can be seen from our results, indicating that, under medium-level ammonia stress, growth of AM-conducting *Methanosarcina* led to faster consumption of acetate, which could be more efficient than the growth of acetate-oxidizing syntrophs to optimize digester performance.

Conclusions

Multiple isotope-tracking strategies quantitatively recorded the gradual transition of AM to SAO-HM with increasing levels of NH_3. Tracking ^{13}C from [^{13}C]$NaHCO_3$ and [2-^{13}C]CH_3COOH generated similar results, and demonstrated that the CO_2 precursor of HM originated from the carbonate system. Therefore, both ^{13}C-labeling methods and natural ^{13}C signature can be used *ex-situ* and *in-situ* to quantify the methanogenic pathways. Diverse microbial taxa were observed to be involved in this transition process: in thermophilic microbiota, various members of *Syntrophaceticus* and *Methanoculleus* outcompeted *Methanosarcina* under stress from NH_3 of 500-2100 mg-N/L; in mesophilic microbiota, *Methanosaeta* was replaced by the AM-conducting *Methanosarcina* and the syntrophs catalyzing SAO-HM with NH_3 of 200-430 mg-N/L; novel members of *Pseudomonas*, *Bacillus*, uncultured Symbiobacteraceae predominated, which in a comparative study, was shown to be common in acetate enrichments. CO_2-fixing bacterial cells were observed with NanoSIMS, showing that this functional guild could also be detected by DNA-SIP. Development of these ammonia-tolerant consortia was accelerated by acclimation.

Funding

This work was supported by the Foundation of State Key Laboratory of Pollution Control and Resource Reuse (Tongji University), China, (No. PCRRC20019), the National Natural Science Foundation of China (No. 51908415).

Acknowledgements

We thank Julien Malherbe for his assistance with the NanoSIMS analysis.

Appendices

Supplementary Information;

DataS1 Methane production process fitted with Gompertz model;

DataS2 Metadata of sequencing datasets and the OTU tables;

DataS3 Comparative study between 5 cases for *Pseudomona*.

References

Balk, M., Weijma, J., Stams, A.J.M., 2002. *Thermotoga lettingae* sp. nov., a novel thermophilic, methanol-degrading bacterium isolated from a thermophilic anaerobic reactor. Int. J. Syst. Evol. Microbiol. 52, 1361–1368.

Bhandari, V., Gupta, R.S., 2014. Molecular signatures for the phylum (class) Thermotogae and a proposal for its division into three orders (Thermotogales, Kosmotogales ord. nov. and Petrotogales ord. nov.) containing four families (Thermotogaceae, Fervidobacteriaceae fam. nov., Kosmotogaceae fam. nov. and Petrotogaceae fam. nov.) and a new genus *Pseudothermotoga* gen. nov. with five new combinations. Antonie Van Leeuwenhoek 105, 143–168.

Bokulich, N.A., Kaehler, B.D., Rideout, J.R., Dillon, M., Bolyen, E., Knight, R., Huttley, G.A., Gregory Caporaso, J., 2018. Optimizing taxonomic classification of marker-gene amplicon sequences with QIIME 2's q2-feature-classifier plugin. Microbiome 6, 90.

Boone, D.R., Liu, Y., Zhao, Z., Balkwill, D.L., Drake, G.R., Stevens, T., Aldrich, H.C., Al, B.E.T., 1995. *Bacillus infernus* sp.nov., an Fe(III)-and Mn(IV)-reducing

anaerobe from the deep terrestrial subsurface. Int. J. Syst. Bacteriol. 441–448.

Chapleur, O., Wu, T.-D., Guerquin-Kern, J.-L., Mazéas, L., Bouchez, T., 2013. SIMSISH technique does not alter the apparent isotopic composition of bacterial cells. PLoS One 8, e77522.

Conrad, R., 2005. Quantification of methanogenic pathways using stable carbon isotopic signatures: a review and a proposal. Org. Geochem. 36, 739–752.

Dai, X., Yan, H., Li, N., He, J., Ding, Y., Dai, L., Dong, B., 2016. Metabolic adaptation of microbial communities to ammonium stress in a high solid anaerobic digester with dewatered sludge. Sci. Rep. 6, 28193.

Daims, H., Stoecker, K., Wagner, M., 2005. Fluorescence in situ hybridization for the detection of prokaryotes. Mol. Microb. Ecol. 213, 239.

De Vrieze, J., De Mulder, T., Matassa, S., Zhou, J., Angenent, L.T., Boon, N., Verstraete, W., 2020. Stochasticity in microbiology: managing unpredictability to reach the sustainable development goals. Microb. Biotechnol. 13, 829–843.

De Vrieze, J., Hennebel, T., Boon, N., Verstraete, W., 2012. *Methanosarcina*: The rediscovered methanogen for heavy duty biomethanation. Bioresour. Technol. 112, 1–9.

Dyksma, S., Jansen, L., Gallert, C., 2020. Syntrophic acetate oxidation replaces acetoclastic methanogenesis during thermophilic digestion of biowaste. Microbiome 8, 105.

Eastin, J.D., Thorne, C.B., 1963. Carbon dioxide fixation in *Bacillus anthracis*. J.

Bacteriol. 85, 410–417.

Fotidis, I.A., Karakashev, D., Angelidaki, I., 2013a. Bioaugmentation with an acetate-oxidising consortium as a tool to tackle ammonia inhibition of anaerobic digestion. Bioresour. Technol. 146, 57–62.

Fotidis, I.A., Karakashev, D., Kotsopoulos, T.A., Martzopoulos, G.G., Angelidaki, I., 2013b. Effect of ammonium and acetate on methanogenic pathway and methanogenic community composition. FEMS Microbiol. Ecol. 83, 38–48.

Goux, X., Calusinska, M., Lemaigre, S., Marynowska, M., Klocke, M., Udelhoven, T., Benizri, E., Delfosse, P., 2015. Microbial community dynamics in replicate anaerobic digesters exposed sequentially to increasing organic loading rate, acidosis, and process recovery. Biotechnol. Biofuels 8, 122.

Hao, L., Bize, A., Conteau, D., Chapleur, O., Courtois, S., Kroff, P., Desmond-Le Quéméner, E., Bouchez, T., Mazéas, L., 2016. New insights into the key microbial phylotypes of anaerobic sludge digesters under different operational conditions. Water Res. 102, 158–169.

Hao, L., Lü, F., Mazéas, L., Desmond-Le Quéméner, E., Madigou, C., Guenne, A., Shao, L., Bouchez, T., He, P., 2015. Stable isotope probing of acetate fed anaerobic batch incubations shows a partial resistance of acetoclastic methanogenesis catalyzed by *Methanosarcina* to sudden increase of ammonia level. Water Res. 69, 90–99.

Hao, L.P., Mazéas, L., Lü, F., Grossin-Debattista, J., He, P.J., Bouchez, T., 2017. Effect

of ammonia on methane production pathways and reaction rates in acetate-fed biogas processes. Water Sci. Technol. 75, 1839–1848.

Hattori, S., 2008. Syntrophic acetate-oxidizing microbes in methanogenic environments. Microbes Environ. 23, 118–127.

Hattori, S., Kamagata, Y., Hanada, S., Shoun, H., 2000. *Thermacetogenium phaeum* gen. nov., sp. nov., a strictly anaerobic , thermophilic , syntrophic acetate-oxidizing bacterium. Int. J. Syst. Evol. Microbiol. 50, 1601–1609.

Ho, D.P., Jensen, P.D., Batstone, D.J., 2013. Methanosarcinaceae and acetate-oxidizing pathways dominate in high-rate thermophilic anaerobic digestion of waste-activated sludge. Appl. Environ. Microbiol. 79, 6491–6500.

Jeon, B.Y., Jung, I.L., Park, D.H., 2012. Enrichment and isolation of CO_2-fixing bacteria with electrochemical reducing power as a sole energy source. J. Environ. Prot. 3, 55–60.

Li, D., Ran, Y., Chen, L., Cao, Q., Li, Z., Liu, X., 2018. Instability diagnosis and syntrophic acetate oxidation during thermophilic digestion of vegetable waste. Water Res. 139, 263–271.

Li, T., Mazéas, L., Sghir, A., Leblon, G., Bouchez, T., 2009. Insights into networks of functional microbes catalysing methanization of cellulose under mesophilic conditions. Environ. Microbiol. 11, 889–904.

Lü, F., Hao, L., Guan, D., Qi, Y., Shao, L., He, P., 2013. Synergetic stress of acids and ammonium on the shift in the methanogenic pathways during thermophilic

anaerobic digestion of organics. Water Res. 47, 2297–2306.

Mosbæk, F., Kjeldal, H., Mulat, D.G., Albertsen, M., Ward, A.J., Feilberg, A., Nielsen, J.L., 2016. Identification of syntrophic acetate-oxidizing bacteria in anaerobic digesters by combined protein-based stable isotope probing and metagenomics. ISME J. 10, 2405–2418.

Müller, B., Sun, L., Schnürer, A., 2013. First insights into the syntrophic acetate-oxidizing bacteria--a genetic study. Microbiologyopen 2, 35–53.

Müller, B., Sun, L., Westerholm, M., Schnürer, A., 2016. Bacterial community composition and *fhs* profiles of low- and high-ammonia biogas digesters reveal novel syntrophic acetate-oxidising bacteria. Biotechnol. Biofuels 9, 48.

Nobu, M.K., Narihiro, T., Rinke, C., Kamagata, Y., Tringe, S.G., Woyke, T., Liu, W.-T., 2015. Microbial dark matter ecogenomics reveals complex synergistic networks in a methanogenic bioreactor. ISME J. 9, 1710–1722.

Pan, X., Zhao, L., Li, C., Angelidaki, I., Lv, N., Ning, J., Cai, G., Zhu, G., 2020. Deep insights into the network of acetate metabolism in anaerobic digestion: focusing on syntrophic acetate oxidation and homoacetogenesis. Water Res. 116774.

Polag, D., May, T., Müller, L., König, H., Jacobi, F., Laukenmann, S., Keppler, F., 2015. Online monitoring of stable carbon isotopes of methane in anaerobic digestion as a new tool for early warning of process instability. Bioresour. Technol. 197, 161–170.

Puig-Castellví, F., Cardona, L., Bureau, C., Bouveresse, D.J.-R., Cordella, C.B.Y.,

Mazéas, L., Rutledge, D.N., Chapleur, O., 2020. Effect of ammonia exposure and acclimation on the performance and the microbiome of anaerobic digestion. Bioresour. Technol. Reports 11, 100488.

Rotaru, A.A., Stryhanyuk, H., Calabrese, F., Hall, P.O.J., Richnow, H.H., Musat, N., Thamdrup, B., Way, B., 2017. Conductive particles enable syntrophic acetate oxidation between Geobacter and Methanosarcina from coastal sediments 49, 1–32.

Schnürer, A., Schink, B., Svensson, B.H., 1996. *Clostridium ultunense* sp. nov., a mesophilic bacterium oxidizing acetate in syntrophic association with a hydrogenotrophic methanogenic bacterium. Int. J. Syst. Bacteriol. 46, 1145–1152.

Shiratori-Takano, H., Akita, K., Yamada, K., Itoh, T., Sugihara, T., Beppu, T., Ueda, K., 2014. Description of *Symbiobacterium ostreiconchae* sp. nov., *Symbiobacterium turbinis* sp. nov. and *Symbiobacterium terraclitae* sp. nov., isolated from shellfish, emended description of the genus *Symbiobacterium* and proposal of Symbio. Int. J. Syst. Evol. Microbiol. 64, 3375–3383.

Söllinger, A., Schwab, C., Weinmaier, T., Loy, A., Tveit, A.T., Schleper, C., Urich, T., 2016. Phylogenetic and genomic analysis of Methanomassiliicoccales in wetlands and animal intestinal tracts reveals clade-specific habitat preferences. FEMS Microbiol. Ecol. 92.

Spona-Friedl, M., Braun, A., Huber, C., Eisenreich, W., Griebler, C., Kappler, A., Elsner, M., 2020. Substrate-dependent CO_2 fixation in heterotrophic bacteria

revealed by stable isotope labelling. FEMS Microbiol. Ecol. 96.

Sun, L., Müller, B., Westerholm, M., Schnürer, A., 2014. Syntrophic acetate oxidation in industrial CSTR biogas digesters. J. Biotechnol. 171, 39–44.

Thauer, R.K., Kaster, A.-K., Seedorf, H., Buckel, W., Hedderich, R., 2008. Methanogenic archaea: ecologically relevant differences in energy conservation. Nat. Rev. Microbiol. 6, 579–591.

Wang, H.-Z., Gou, M., Yi, Y., Xia, Z.-Y., Tang, Y.-Q., 2018. Identification of novel potential acetate-oxidizing bacteria in an acetate-fed methanogenic chemostat based on DNA stable isotope probing. J. Gen. Appl. Microbiol. 64, 221–231.

Watsuji, T., Kato, T., Ueda, K., Beppu, T., Atsuji, T.W., Ato, T.K., Eda, K.U., Eppu, T.B., 2006. CO_2 supply induces the growth of Symbiobacterium thermophilum , a syntrophic bacterium. Biosci. Biotechnol. Biochem. 70, 753–756.

Werner, J.J., Garcia, M.L., Perkins, S.D., Yarasheski, K.E., Smith, S.R., Muegge, B.D., Stadermann, F.J., DeRito, C.M., Floss, C., Madsen, E.L., Gordon, J.I., Angenent, L.T., 2014. Microbial community dynamics and stability during an ammonia-induced shift to syntrophic acetate oxidation. Appl. Environ. Microbiol. 80, 3375–3383.

Westerholm, M., Dolfing, J., Schnürer, A., 2019. Growth characteristics and thermodynamics of syntrophic acetate oxidizers. Environ. Sci. Technol. 53, 5512–5520.

Westerholm, M., Levén, L., Schnürer, A., 2012. Bioaugmentation of syntrophic

1 acetate-oxidizing culture in biogas reactors exposed to increasing levels of
2 ammonia. Appl. Environ. Microbiol. 78, 7619–7625.

3 Westerholm, M., Müller, B., Isaksson, S., Schnürer, A., 2015. Trace element and
4 temperature effects on microbial communities and links to biogas digester
5 performance at high ammonia levels. Biotechnol. Biofuels 8, 154.

6 Westerholm, M., Müller, B., Singh, A., Karlsson Lindsjö, O., Schnürer, A., 2018.
7 Detection of novel syntrophic acetate-oxidizing bacteria from biogas processes by
8 continuous acetate enrichment approaches. Microb. Biotechnol. 11, 680–693.

9 Westerholm, M., Roos, S., Schnürer, A., 2011. *Tepidanaerobacter acetatoxydans* sp.
10 nov., an anaerobic, syntrophic acetate-oxidizing bacterium isolated from two
11 ammonium-enriched mesophilic methanogenic processes. Syst. Appl. Microbiol.
12 34, 260–266.

13 Westerholm, M., Roos, S., Schnürer, A., 2010. *Syntrophaceticus schinkii* gen. nov., sp.
14 nov., an anaerobic, syntrophic acetate-oxidizing bacterium isolated from a
15 mesophilic anaerobic filter. FEMS Microbiol. Lett. 309, 100–104.

16 Whiticar, M.J., Faber, E., Schoell, M., 1986. Biogenic methane formation in marine
17 and freshwater environments: CO_2 reduction vs. acetate fermentation—Isotope
18 evidence. Geochim. Cosmochim. Acta 50, 693–709.

19 Xiao, Y., Hui, W., Wang, Q., Roh, S.W., Shi, X., Shi, J., Quan, Z., 2009. *Pseudomonas*
20 *caeni* sp . nov ., a denitrifying bacterium isolated from the sludge of an anaerobic
21 ammonium-oxidizing bioreactor. Int. J. Syst. Evol. Microbiol. 2594–2598.

Zheng, D., Wang, H.-Z., Gou, M., Nobu, M.K., Narihiro, T., Hu, B., Nie, Y., Tang, Y.-Q., 2019. Identification of novel potential acetate-oxidizing bacteria in thermophilic methanogenic chemostats by DNA stable isotope probing. Appl. Microbiol. Biotechnol. 103, 8631–8645.

Zwietering, M.H., Jongenburger, I., Rombouts, F.M., van't Riet, K., 1990. Modeling of the Bacterial Growth Curve. Appl. Environ. Microbiol. 56, 1875–1881.

Figure captions

Figure 1 Schematic of experimental set up. Details are given in **Table S1**.

Figure 2 Methane production and acetate consumption by microbiota during 110-day batch incubation with acetate at a rate of 110 mmol/L. The modified Gompertz three-parameter model was fitted to the experimentally recorded cumulative CH_4 production curves as detailed in **Supplementary Section 1.4** and **DataS1**. Inoculated microbiota originating from mesophilic or thermophilic reactors were incubated at 35 °C (a-b, e-f) or 55 °C (c-d, g-h). NH_4Cl was added to reach NH_4^+-N of 0.14 g/L in (a, c, e, g), 5.00 g/L in (b, f) and 7.00 g/L in (d, h). Acclimated and non-acclimated microbiota were used as inocula in (a-d) and (e-h), which were respectively pre-exposed to NH_4^+-N of 5.00 g/L (in the mesophilic treatment) or 7.00 g/L (in the thermophilic treatment) and 0.14 g/L (for both) before this batch test. Details on reactor settings are given in **Table S1**. Acetate concentration was only analysed for 2-4 representative reactors of each set showing diverged methane production curves.

Figure 3 Tracking stable carbon isotope in the biogas to quantify the contribution of methane production pathways using three different ^{13}C-labeling strategies. ^{13}C composition in CH_4 ($\Delta^{13}CH_4$) and CO_2 ($\Delta^{13}CO_2$) of the biogas were monitored in reactor r3 fed with [2-^{13}C] CH_3COOH (a-d) and reactor r5 fed with [^{13}C] $NaHCO_3$ (e-h), and the natural ^{13}C signature in CH_4 ($\delta^{13}CH_4$) and CO_2 ($\delta^{13}CO_2$) was monitored in reactors r1 and r2 fed with unlabeled compounds (i-l). The percentage contribution of syntrophic acetate oxidation coupled with hydrogenotrophic methanogenesis ($f_{SAO\text{-}HM}$) was calculated with $\Delta^{13}CH_4$ and $\Delta^{13}CO_2$ (m-p), and the apparent stable carbon isotope fractionation factor (α_c) was calculated with $\delta^{13}CH_4$ and $\delta^{13}CO_2$ (q-t). Microbiota MA and MnA or TA and TnA were incubated at 35 °C (a-b, e-f, i-j, m-n, q-r) or 55 °C (c-d, g-h, o-p, s-t) with NH_4^+-N of 0.14 g/L in (a, c, e, g, i, k, m, o, q, s), 5.00 g/L in (b, f, j, n, r) and 7.00 g/L in (d, h, l, p, t).

Figure 4 16S rRNA gene copy numbers of (a, d) *Methanoculleus*, (b, e) *Methanosarcina* and (c, f) Methanosaetaceae alongside methane production in mesophilic reactors MA-H-r4, -r5, MnA-H-r4, -r5 (a-c), and thermophilic reactors TA-H-r4, -r5, TnA-H-r4, -r5 (d-f). More information is given in **Figure S2**.

Figure 5 FISH images showing the development of acetate-oxidizing syntrophs from microbiota initially dominated by acetotrophic methanogens in mesophilic conditions with NH_4^+-N at a rate of 5 g/ (a-f) or in thermophilic conditions with NH_4^+-N a rate of 7 g/L (g-l). Legends on the images

give the name of the reactor and the time of sampling during the incubation. In (a-f, h-i, k-l), a mixture of probes was used, including Archaea-specific Arc915 (FLUO-labeled, green), Methanomicrobiales-specific MG1200 (Cy5-labeled, blue), Methanosarcinaceae-specific MS1414 (Cy3-labeled, red) and Bacteria-specific EUB338 (Cy3-labeled, red); the targeted cells of Methanomicrobiales and Methanosarcinaceae appear in light blue and yellow respectively, other archaeal cells appear in green and bacterial cells are in red. The green rod-shaped cells were demonstrated to be Methanosaetaceae, as shown in **Figure S3**. In (g, j), probes including Archaea-specific Arc915 (FLUO-labeled, green), Methanosarcinaceae-specific MS1414 (Cy5-labeled, blue) and Methanosaetaceae-specific Mx825 (Cy3-labeled, red) were used. The targeted cells of Methanosarcinaceae and Methanosaetaceae are in respectively, light blue and yellow; other archaeal cells are in green. Details are given in **Supplementary Methods Section 1.6**.

Figure 6 (a) The 40 most abundant bacterial OTUs, (b) 20 most abundant archaeal OTUs and (c) 8 most abundant OTUs of known or candidate syntrophic acetate oxidizing bacteria (with relative abundance < 1%) in the microbial communities of the heavy and light DNA fractions derived from the ^{13}C and ^{15}N co-probing experiments conducted in reactor r4 with high ammonium levels. The biomass samples used for DNA extraction were taken on Day 89 for MnA and TnA, Day 67 for MA, and Day 46 for TA when methanogenesis recovered from the last lag phase during incubation. Separation of the heavy (_H) and light (_L) DNA fractions is shown in **Figure S5**. Labels at the top of the heatmap show the incubation temperature. Labels at the bottom show the condition of the reactor and the DNA fraction. Reactor conditions include: MA for mesophilic acclimated microbiota; MnA for mesophilic non-acclimated microbiota; TA for thermophilic acclimated microbiota; TnA for thermophilic non-acclimated microbiota. "_H" and "_L" represent the heavy and light DNA fractions, respectively. Genus and species level information is given in **Figure S6** and **S7**.

Figure 7 NanoSIMS images showing the enrichment in ^{13}C and ^{15}N by bacterial cells in a sample incubated with [^{13}C]$NaHCO_3$ and [^{15}N]NH_4Cl after 81 days in MA-H-r5 fed with CH_3COOH of 110 mmol/L at NH_4^+-N of 5.00 g/L. (a-h) represent the same field of observation. (a-d, g-h) show the secondary ion species targeted. In particular, "^{81}Br" indicates signal from bacterial cells pre-hybridized with the brominated EUB338 bacterial probe. (e-f) show percentage abundance of ^{13}C and ^{15}N in the cells, calculated with Eq.S3 and Eq.S4; each color in the color scale corresponds to a 1% or 6% increment in (e) and (f) respectively, detailed data are provided in **Figure S10**. (i) is a FISH observation of the same sample; arrows point to spherical cells of Methanomicrobiales (blue) pre-hybridized with MG1200-Cy5 and ARC915-FLUO, which were loosely assembled with the rod-

shape bacterial cells (red) hybridized with EUB338-Cy3, similar to the assembles in (a-h). The scale bar equals 5 μm.

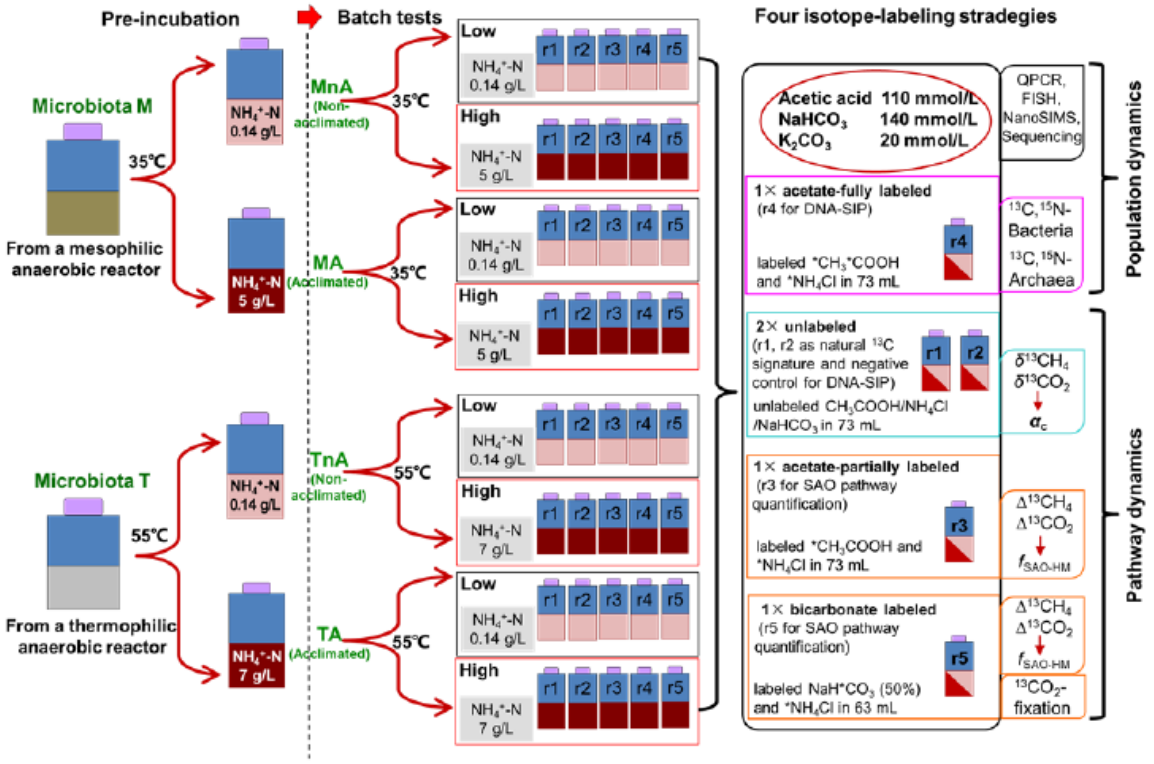

Figure 1 Schematic of experimental set up. Details are given in **Table S1**.

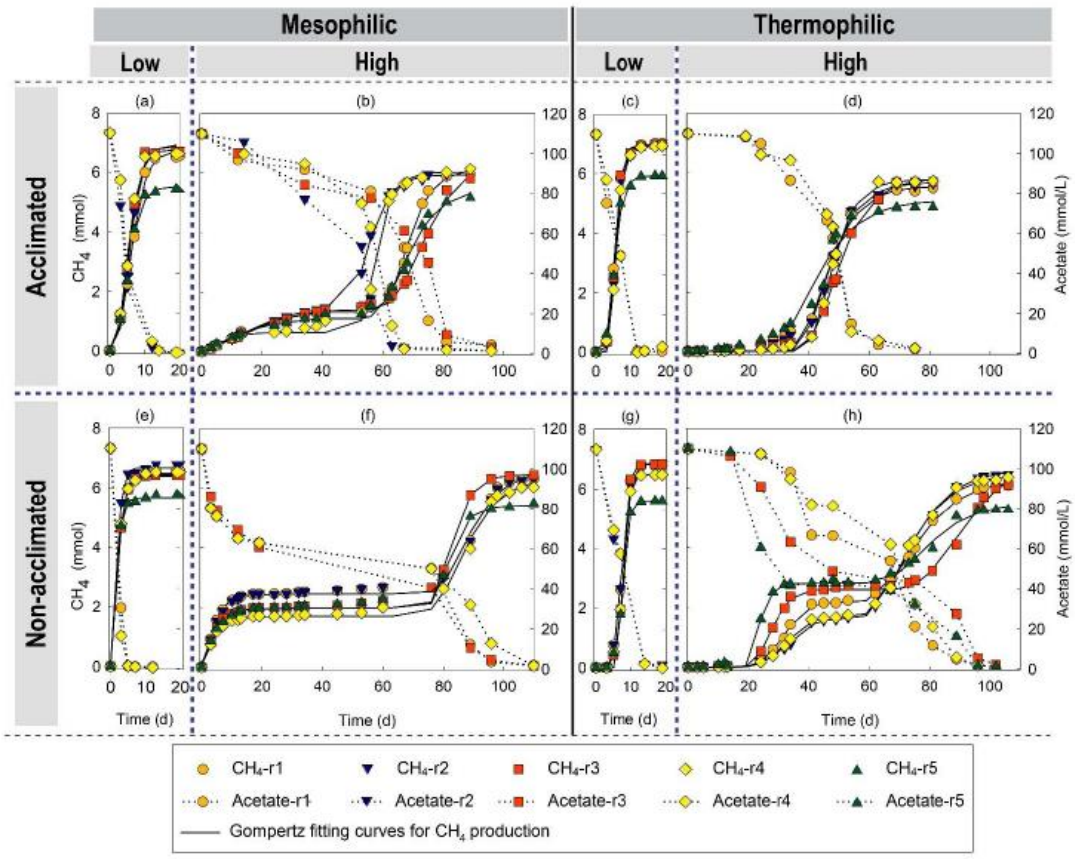

Figure 2 Methane production and acetate consumption by microbiota during 110-day batch incubation with acetate at a rate of 110 mmol/L. The modified Gompertz three-parameter model was fitted to the experimentally recorded cumulative CH_4 production curves as detailed in **Supplementary Section 1.4** and **DataS1**. Inoculated microbiota originating from mesophilic or thermophilic reactors were incubated at 35 °C (a-b, e-f) or 55 °C (c-d, g-h). NH_4Cl was added to reach NH_4^+-N of 0.14 g/L in (a, c, e, g), 5.00 g/L in (b, f) and 7.00 g/L in (d, h). Acclimated and non-acclimated microbiota were used as inocula in (a-d) and (e-h), which were respectively pre-exposed to NH_4^+-N of 5.00 g/L (in the mesophilic treatment) or 7.00 g/L (in the thermophilic treatment) and 0.14 g/L (for both) before this batch test. Details on reactor settings are given in **Table S1**. Acetate concentration was only analysed for 2-4 representative reactors of each set showing diverged methane production curves.

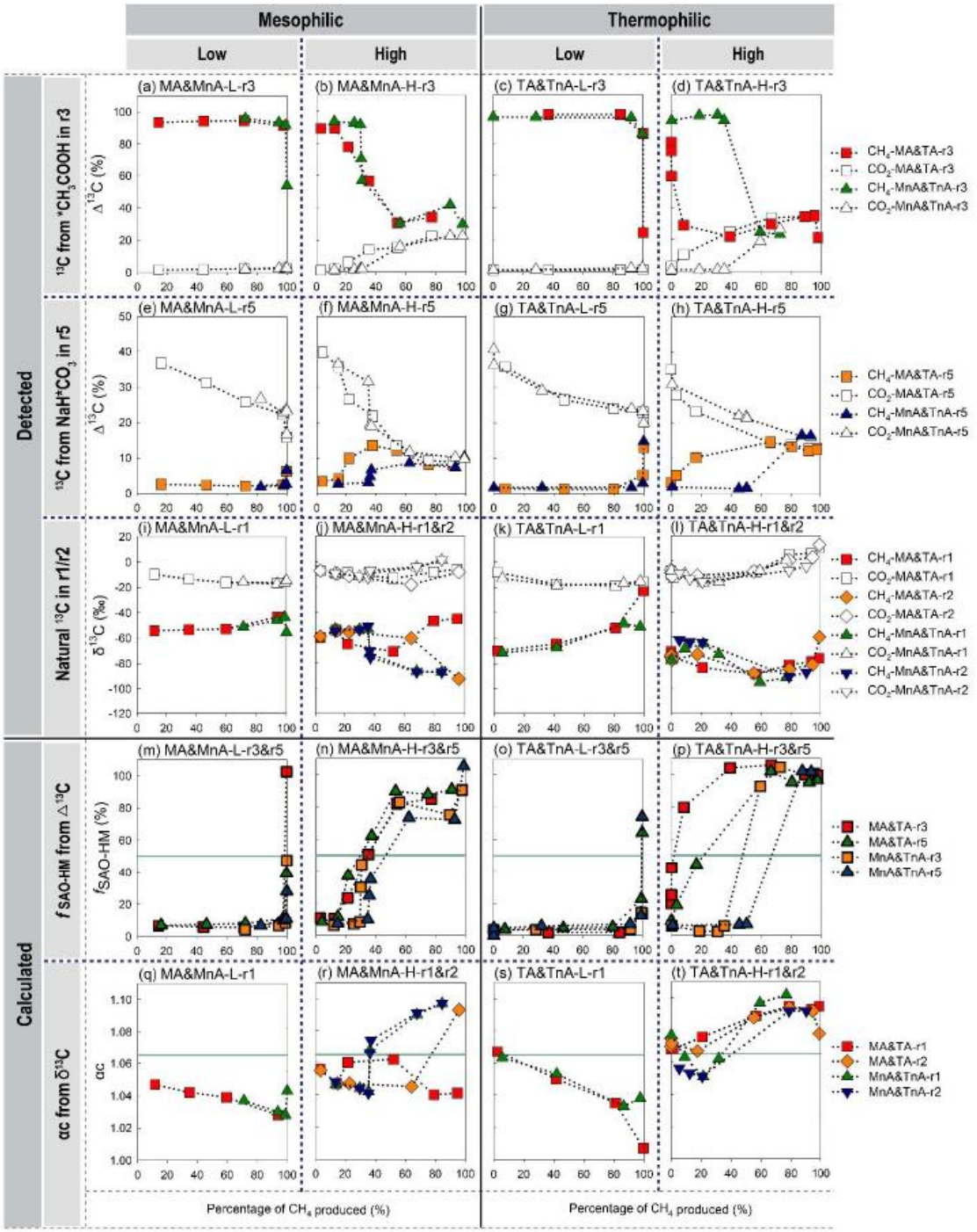

Figure 3 Tracking stable carbon isotope in the biogas to quantify the contribution of methane production pathways using three different ^{13}C-labeling strategies. ^{13}C composition in CH_4

($\Delta^{13}CH_4$) and CO_2 ($\Delta^{13}CO_2$) of the biogas were monitored in reactor r3 fed with [2-^{13}C] CH_3COOH (a-d) and reactor r5 fed with [^{13}C] $NaHCO_3$ (e-h), and the natural ^{13}C signature in CH_4 ($\delta^{13}CH_4$) and CO_2 ($\delta^{13}CO_2$) was monitored in reactors r1 and r2 fed with unlabeled compounds (i-l). The percentage contribution of syntrophic acetate oxidation coupled with hydrogenotrophic methanogenesis ($f_{SAO\text{-}HM}$) was calculated with $\Delta^{13}CH_4$ and $\Delta^{13}CO_2$ (m-p), and the apparent stable carbon isotope fractionation factor (α_c) was calculated with $\delta^{13}CH_4$ and $\delta^{13}CO_2$ (q-t). Microbiota MA and MnA or TA and TnA were incubated at 35 °C (a-b, e-f, i-j, m-n, q-r) or 55 °C (c-d, g-h, o-p, s-t) with NH_4^+-N of 0.14 g/L in (a, c, e, g, i, k, m, o, q, s), 5.00 g/L in (b, f, j, n, r) and 7.00 g/L in (d, h, l, p, t).

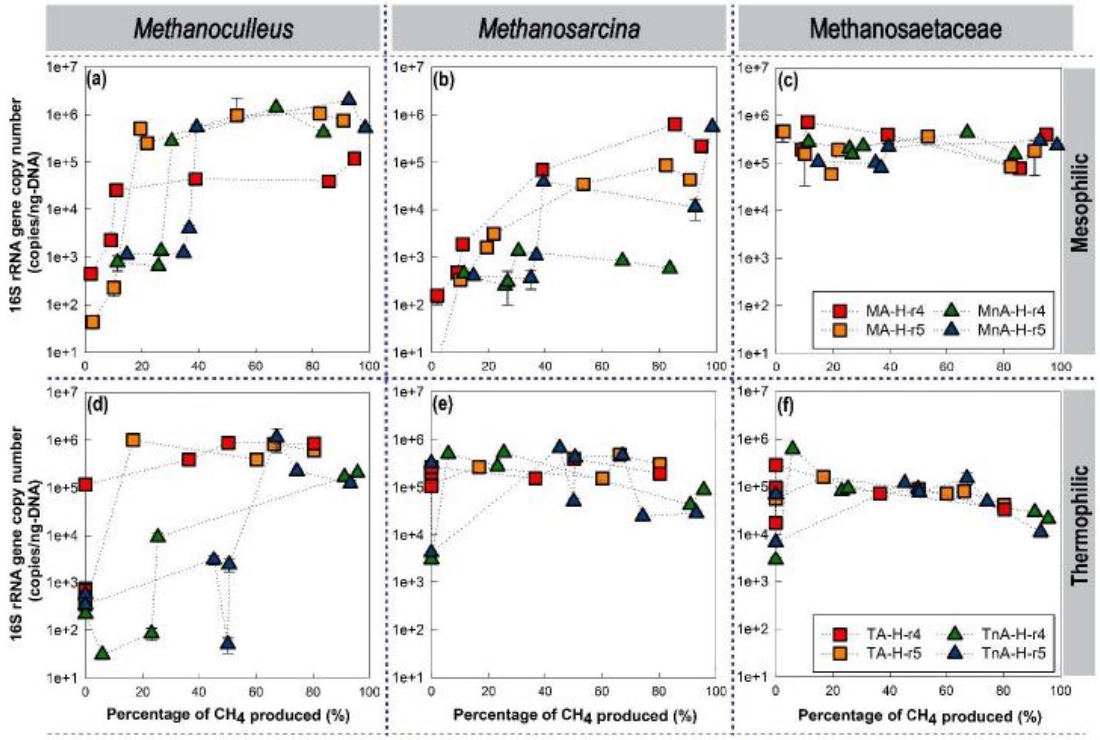

Figure 4 16S rRNA gene copy numbers of (a, d) *Methanoculleus*, (b, e) *Methanosarcina* and (c, f) Methanosaetaceae alongside methane production in mesophilic reactors MA-H-r4, -r5, MnA-H-r4, -r5 (a-c), and thermophilic reactors TA-H-r4, -r5, TnA-H-r4, -r5 (d-f). More information is given in **Figure S2**.

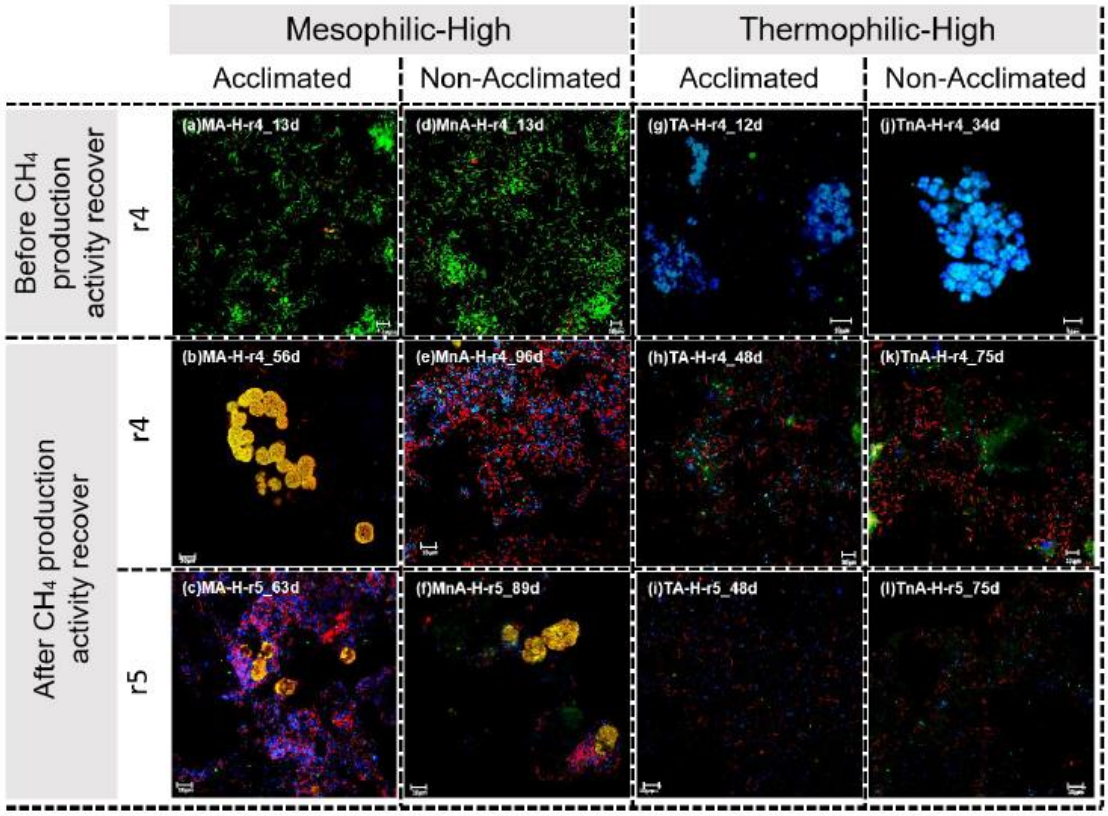

Figure 5 FISH images showing the development of acetate-oxidizing syntrophs from microbiota initially dominated by acetotrophic methanogens in mesophilic conditions with NH_4^+-N at a rate of 5 g/ (a-f) or in thermophilic conditions with NH_4^+-N a rate of 7 g/L (g-l). Legends on the images give the name of the reactor and the time of sampling during the incubation. In (a-f, h-i, k-l), a mixture of probes was used, including Archaea-specific Arc915 (FLUO-labeled, green), Methanomicrobiales-specific MG1200 (Cy5-labeled, blue), Methanosarcinaceae-specific MS1414 (Cy3-labeled, red) and Bacteria-specific EUB338 (Cy3-labeled, red); the targeted cells of Methanomicrobiales and Methanosarcinaceae appear in light blue and yellow respectively, other archaeal cells appear in green and bacterial cells are in red. The green rod-shaped cells were demonstrated to be Methanosaetaceae, as shown in **Figure S3**. In (g, j), probes including Archaea-specific Arc915 (FLUO-labeled, green), Methanosarcinaceae-specific MS1414 (Cy5-labeled, blue) and Methanosaetaceae-specific Mx825 (Cy3-labeled, red) were used. The targeted cells of Methanosarcinaceae and Methanosaetaceae are in respectively, light blue and yellow; other archaeal cells are in green. Details are given in **Supplementary Methods Section 1.6**.

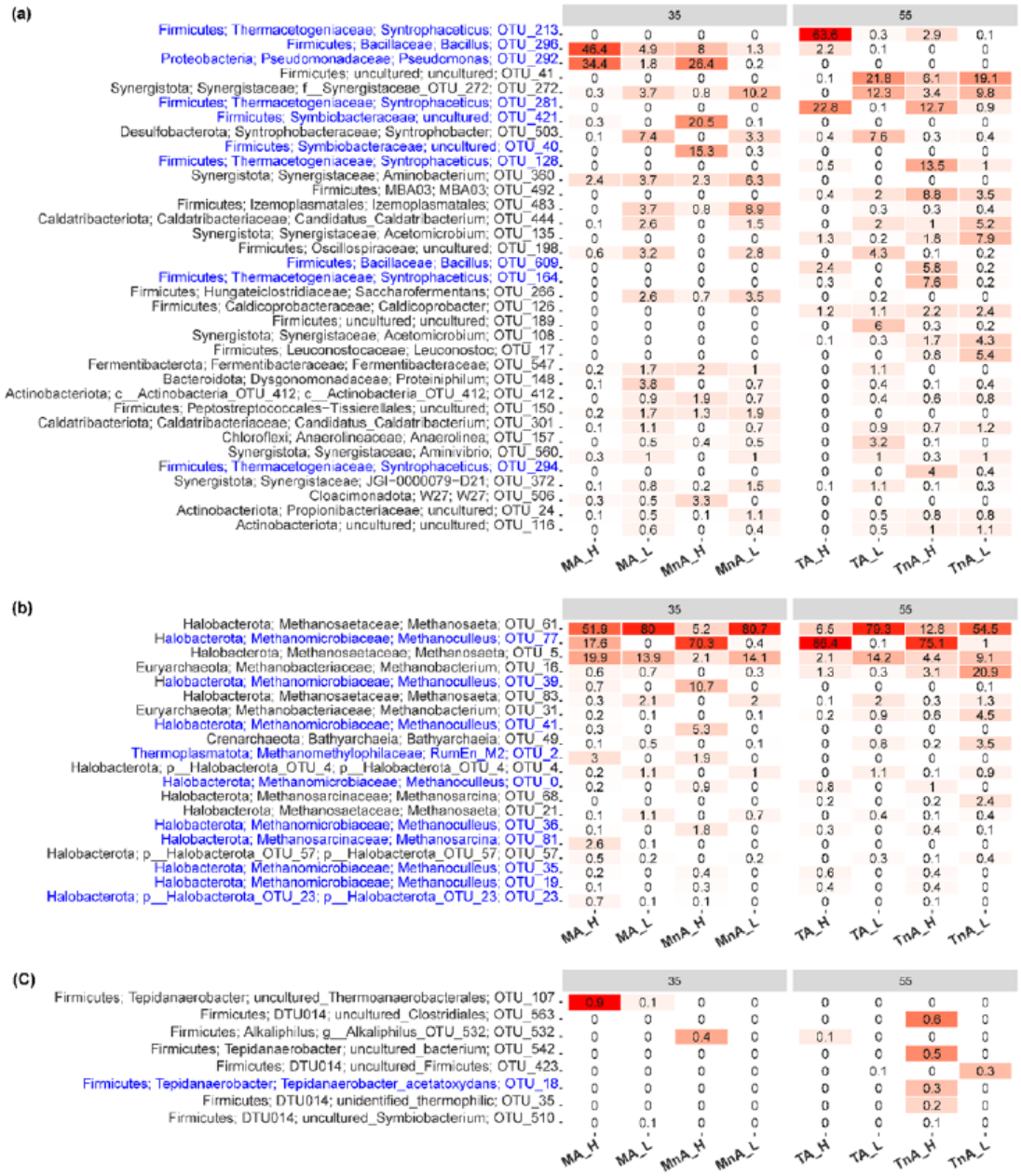

Figure 6 (a) The 40 most abundant bacterial OTUs, (b) 20 most abundant archaeal OTUs and (c) 8 most abundant OTUs of known or candidate syntrophic acetate oxidizing bacteria (with relative abundance < 1%) in the microbial communities of the heavy and light DNA fractions derived from the ^{13}C and ^{15}N co-probing experiments conducted in reactor r4 with high ammonium levels. The biomass samples used for DNA extraction were taken on Day 89 for MnA and TnA, Day 67 for

MA, and Day 46 for TA when methanogenesis recovered from the last lag phase during incubation. Separation of the heavy (_H) and light (_L) DNA fractions is shown in **Figure S5**. Labels at the top of the heatmap show the incubation temperature. Labels at the bottom show the condition of the reactor and the DNA fraction. Reactor conditions include: MA for mesophilic acclimated microbiota; MnA for mesophilic non-acclimated microbiota; TA for thermophilic acclimated microbiota; TnA for thermophilic non-acclimated microbiota. "_H" and "_L" represent the heavy and light DNA fractions, respectively. Genus and species level information is given in **Figure S6** and **S7**.

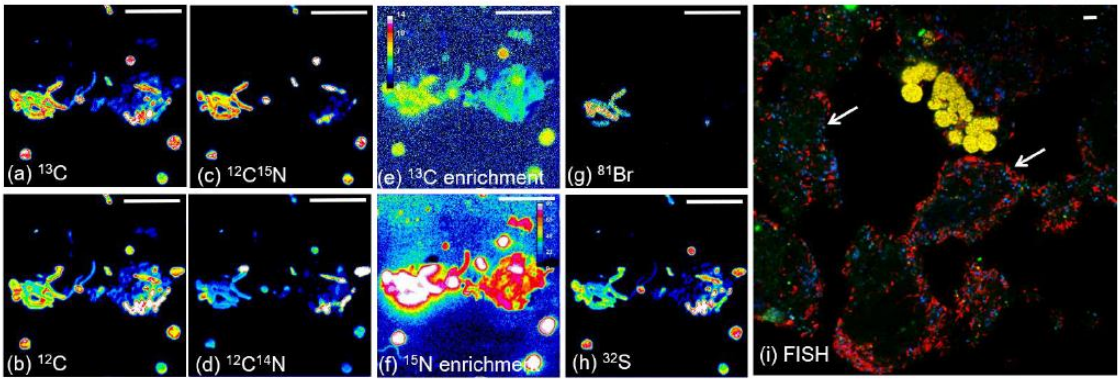

Figure 7 NanoSIMS images showing the enrichment in ^{13}C and ^{15}N by bacterial cells in a sample incubated with [^{13}C]NaHCO$_3$ and [^{15}N]NH$_4$Cl after 81 days in MA-H-r5 fed with CH_3COOH of 110 mmol/L at NH_4^+-N of 5.00 g/L. (a-h) represent the same field of observation. (a-d, g-h) show the secondary ion species targeted. In particular, "^{81}Br" indicates signal from bacterial cells pre-hybridized with the brominated EUB338 bacterial probe. (e-f) show percentage abundance of ^{13}C and ^{15}N in the cells, calculated with Eq.S3 and Eq.S4; each color in the color scale corresponds to a 1% or 6% increment in (e) and (f) respectively, detailed data are provided in **Figure S10**. (i) is a FISH observation of the same sample; arrows point to spherical cells of Methanomicrobiales (blue) pre-hybridized with MG1200-Cy5 and ARC915-FLUO, which were loosely assembled with the rod-shape bacterial cells (red) hybridized with EUB338-Cy3, similar to the assembles in (a-h). The scale bar equals 5 μm.